ADVANCED OPTICAL MATERIALS
www.advopticalmat.de

Independent Tailoring of Super-Radiant and Sub-Radiant Modes in High-*Q* Plasmonic Fano Resonant Metasurfaces

*Govind Dayal, Xin Yu Chin, Cesare Soci, and Ranjan Singh**

Fano resonances in plasmonic metasurfaces arise from the interference between a super-radiant and a sub-radiant plasmon mode. The interference of the plasmon modes, which gives rise to the Fano resonance phenomenon in a plasmonic metasurface, also restricts the independent control of the individual resonance modes. Independent tailoring of super-radiant and sub-radiant plasmon modes at nanoscale is one of the challenges to be addressed for the realization of targeted functionalities and fundamental understanding of plasmon mode coupling. Here, it is experimentally and numerically shown that the spectral position and line-width of both the super-radiant and sub-radiant plasmonic modes of a Fano resonance can be independently controlled through the variation of metal film thickness at the skin depth scale and polarization of the incident light. The metasurface consists of a conductively coupled annular and rectangular aperture array that supports multiple high-*Q* Fano resonances at near-infrared frequencies. Fano resonances are excited via interference between the azimuthal plasmon mode of the annular aperture and the dipolar plasmon mode of the rectangular aperture. The multiple Fano resonances excited in the proposed design show remarkable sensitivity to skin-depth scale film thicknesses, enabling independent control of spectral position and line-shape of super-radiant and sub-radiant modes in high-*Q* plasmonic Fano resonant metasurfaces.

1. Introduction

The ability of plasmonic nanostructures to concentrate incident radiation well below the diffraction limit offers unique possibilities for controlling and manipulating light at sub-wavelength scale.[1,2] These unique functionalities are enabled by the excitation of coherent oscillations of free electrons in the finite sized nanostructure driven by the incident electric field of the electromagnetic wave, known as localized surface plasmon resonances.[3–6] The intense electromagnetic field near the edges of nanostructures at plasmon resonances known to be "hot spots" has become an ideal candidate for surface-enhanced Raman spectroscopy, surface-enhanced florescence, and surface-enhanced infrared absorption spectroscopy, which utilizes the field enhancement properties of metal nanostructures to detect the signal from a single molecule.[7–9] The largest possible field enhancement depends on the quality factor (*Q*) of the resonances. Wang et al. have shown that the *Q*-factor of the plasmon resonance depends only on the dielectric function of the metal at a given plasmon frequency but not on the geometric form and shape of the nanostructure.[10] The maximum possible *Q*-factor for a metal nanostructure is limited by the ratio of real and imaginary parts of dielectric function of the metals, and is less than 10–20 in the visible and near IR.[11] The spectral response of these localized surface plasmon resonances does not depend only on their size and shape, but also on their dielectric environment. In the quasi-static limit, free electrons in the metal nanostructure experience spatially homogeneous field with roughly the same phase of the incident electromagnetic field, leading to the excitation of a dipole resonance.[2,3] In addition to the dipole resonance, quadrupole and higher order modes can also be observed. The higher order modes (quadrupole, octupole, etc.) of the sub-wavelength sized plasmonic nanostructures do not directly couple to the incident radiation at normal incidence. However, these modes can be excited at normal incidence (nonretarded case) through asymmetric coupling by breaking the structural symmetry or at an oblique angle of incidence illumination (retarded case).[3] Interesting phenomena arise when the plasmon modes start interfering with each other resulting in a completely new kind of resonances, e.g., Fano resonance. Fano resonances are characterized by a distinct asymmetric line shape, which originates from the interference of a broad spectral background state and a narrow discrete state.[12] Ugo Fano explained the asymmetric shape of such spectral lines based on the superposition between two scattering channels involving a continuum and a discrete state with an asymmetric line shape given by

$$S(\varepsilon) = (F\gamma + \omega - \omega_0)^2 / (\omega - \omega_0)^2 + \gamma^2 \quad (1)$$

where ω_0 and γ denote the spectral resonance position and line-width of the resonance, respectively; F is the so-called

Dr. G. Dayal, X. Y. Chin, Prof. C. Soci, Prof. R. Singh
Center for Disruptive Photonic Technologies
The Photonics Institute
Nanyang Technological University
50 Nanyang Avenue, Singapore 639798
Division of Physics and Applied Physics
School of Physical and Mathematical Sciences
Nanyang Technological University
21 Nanyang Link, Singapore 637371
E-mail: ranjans@ntu.edu.sg

DOI: 10.1002/adom.201600417

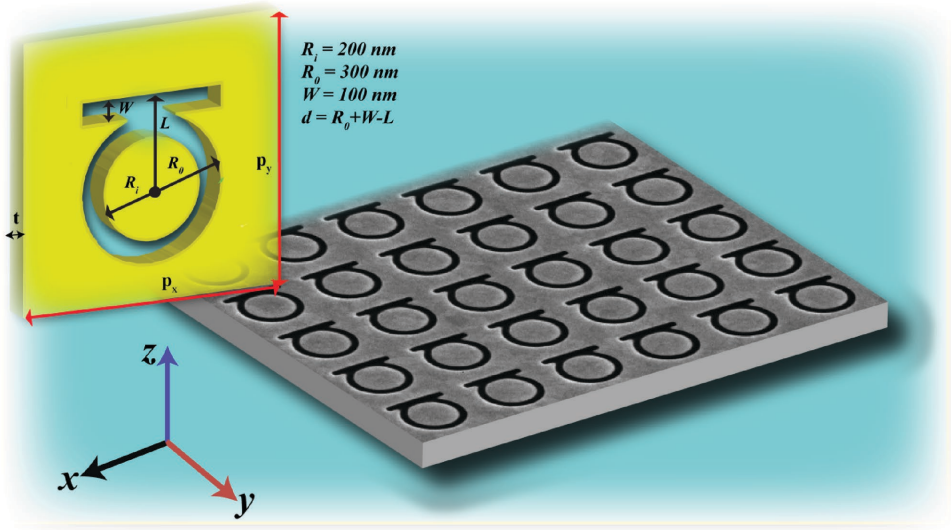

Figure 1. SEM image of 2D array of the overlapping annular and rectangular apertures fabricated by focused ion beam. The inner and outer diameters of the annular aperture are 400 and 600 nm, respectively. The periodicity in both *x*- and *y*-directions is 800 nm. A schematic diagram of the unit cell with the geometric definitions is shown in the inset.

Fano parameter, which describes the degree of asymmetry.[13] A simplified form of the Fano formula can be represented as a product of a broad parabolic curve and a narrow Lorentzian curve

$$S(\varepsilon) = ((F\gamma + \omega - \omega_0)^2) * (1/((\omega - \omega_0)^2 + \gamma^2)) \quad (2)$$

From the above expression, it can be clearly seen that it is not necessary to have a continuum state to excite a Fano resonance, rather this can also be achieved upon interference of the two modes resonant at the same frequency, but with contrasting ***Q*** values.

Engineering of Fano resonances in plasmonic systems has experienced tremendous growth in the past decade due to the emergence of plasmonic metasurfaces, whose electromagnetic properties can be tailored to meet specific on-demand applications in a way that is unaffordable with natural materials.[14–16] In a plasmonic system, the continuum state of radiative waves can be constructed from the dipolar (super-radiant) mode and the discrete state can be constructed from the higher-order (sub-radiant) mode of a properly designed plasmonic nanostructure.[17] The interference of plasmon modes, which provide the mechanism for Fano resonance excitation, is obtained via symmetry breaking to generate plasmonic Fano resonances for various nanostructures constructed from disk-ring cavities,[18–20] metal nanostructure heptamers,[21] pentamers,[22] quadrumers,[23] dolmen structures,[24] and asymmetric split ring resonators[25–27]. The importance of Fano resonance in plasmonic systems stem from the fact that it gives rise to sharp resonances in the optical and near-infrared frequency regime, which is otherwise challenging due to inherent dissipative losses in the plasmonic materials. The sharp spectral feature of Fano resonance and consequently the enhanced optical field have been used for a variety of applications including second harmonic generation, plasmonic rulers, refractive index sensors, and biosensors.[28–32]

Unfortunately, as the Fano resonance is built upon a collective effect, it is arduous to independently control the individual sub-radiant and the super-radiant resonances without any mutual influence.[33,34] In this manuscript, we experimentally and numerically show that the spectral position and the linewidth of both the super-radiant and sub-radiant modes of the Fano resonance can be independently controlled through the variation in metal film thickness at the skin-depth scale and polarization of the incident light. The independent control of super-radiant and sub-radiant modes of the Fano resonance through the metal film thickness is enabled by appropriate engineering of the plasmonic metasurface that consists of conductively coupled annular and rectangular aperture arrays. The two resonators that spectrally and spatially overlap give rise to sub-radiant Fano resonances with strong thickness-dependent optical response. The super-radiant mode of the coupled system is the dipolar mode of the annular aperture, which is independent of the film thickness.

A schematic diagram of the metasurface, consisting of conductively coupled annular and rectangular apertures are shown in **Figure 1**. The super-radiant modes of the individual annular aperture and the rectangular aperture are engineered to spectrally and spatially overlap to build Fano-like resonances in plasmonic nanostructures. The sub-radiant mode, which provides the mechanism for Fano resonance generation, is obtained via symmetry breaking. Arrays of overlapping annular and rectangular apertures were fabricated by focused ion beam milling in 50 and 100 nm thick gold films deposited on a quartz substrate. Arrays have been created using a square lattice with a fixed period of 800 nm. The overlap distance between annular and rectangular apertures is varied in the range of 20–60 nm. The top view of scanning electron microscopy (SEM) image of the overlapping annular and rectangular apertures is shown in Figure 1. The inner and outer diameters of the annular apertures are 400 and 600 nm, respectively, and the length and width of the rectangular apertures are 600 and 100 nm,

Adv. Optical Mater. **2016**,
DOI: 10.1002/adom.201600417

respectively. The size of each fabrication area has a footprint of 35 μm × 35 μm.

Reflection spectra were obtained with a Fourier transform infrared spectrometer (Bruker Vertex 80) equipped with a confocal microscope (Hyperion 1000), including a liquid nitrogen-cooled mercury cadmium telluride detector. The zeroth order of the reflected light is collected with a 0.5 NA objective. The illumination light is focused onto the sample at a quasinormal (≈10°) incidence. All the spectra are recorded with a resolution of 4 cm^{-1} and 128 scans. The state of polarization of the incident light was controlled using a ZnSe polarizer. All measurements are normalized with respect to the reflectance from a plain gold mirror.

2. Results and Discussion

In **Figure 2**, we present the measured reflection spectra from 50 nm (top panel) and 100 nm (bottom panel) metal film perforated with a 2D square array of overlapping annular and rectangular aperture having different overlapping distance '*d*'. In Figure 2, the dotted curves show reflection spectra for the *x*-polarization i.e., electric field polarized parallel to the length of the rectangular aperture, while solid curves represent the reflection spectra for the *y*-polarization i.e., electric field polarized perpendicular to the length of the rectangular aperture. As shown in Figure 2, the reflection properties of the structure depend strongly on both the metal thickness as well as on the polarization state of incident electromagnetic wave. We begin our analysis by comparing the measured reflection spectra of 50 and 100 nm thick metal films perforated with an array of overlapping annular and rectangular apertures having a fixed overlap distance of 20 nm. For the case of 50 nm film thickness, the measured reflection spectrum (dotted black curve) for *x*-polarization reveals a broad resonance at 130 THz accompanied by two sharp reflection dips at 169 and 216 THz, respectively, as shown in Figure 2a. It will be shown in the electric field plots later that the broad resonance with a reflection dip at 130 THz is due to the excitation of the azimuthal dipole mode ($m = 2$) in the annular aperture and the two pronounced dips at 169 and 216 THz are due to the formation of the Fano resonances resulting from the interference of the azimuthal quadrupolar mode ($m = 4$) of the annular aperture with the dipolar and quadrupolar modes of the rectangular aperture. For the identical structure with 100 nm metal film thickness, the broad dipolar (super-radiant) resonance ($m = 2$) appears at the same spectral position (130 THz), while the Fano resonances are blue-shifted to 185 and 223 THz, respectively, as shown in Figure 2d (dotted black curve). Next, we compare the reflection spectra of the same structure for *y*-polarization. The measured reflection spectrum obtained for *y*-polarization (solid red curve in Figure 2a) shows a broad resonance at 155 THz, with a Fano resonance at 172 THz, while the reflection spectrum obtained from 100 nm thick film shows a comparatively narrower fundamental ($m = 2$) resonance at 155 THz with two Fano resonances at 187 and 223 THz, respectively. It is striking to note that for a particular polarization, the fundamental dipolar mode ($m = 2$) appears at the same spectral position for both metal thicknesses (50 and 100 nm), while the Fano resonances are blue-shifted with increasing film thickness. This indicates that the Fano resonances are strongly dependent on the film thickness, while the fundamental dipolar resonance is independent of film thickness. Furthermore, it is noted that the Fano resonances excited in 100 nm thick metal film appear at almost the same frequencies for both the *x*- and *y*-polarizations while the fundamental ($m = 2$) mode is strongly polarization dependent and appears at different resonance frequencies. This allows us to independently control the dipolar mode and the Fano resonances in

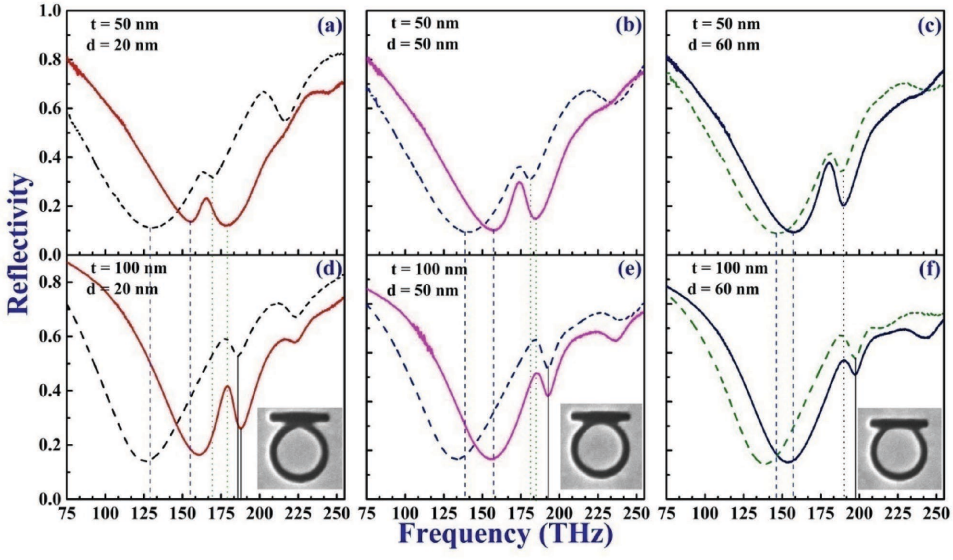

Figure 2. Measured reflection spectra for different overlap distances between annular and rectangular aperture under normal illumination with the electric field component along *x*-(dotted curves) and *y*-(solid curves) directions. Top panels (a–c) shows the reflection spectra for 50 nm thick film and bottom panels (d–f) shows the reflection spectra for 100 nm thick film, respectively. Inset shows unit cell of the metasurface design with overlap between annular and rectangular apertures. The lines in the spectrum are marked to show the spectral separation of the resonances for different thicknesses.

the plasmonic metasurface with the polarization of the incident light and by varying the thickness of the metal film. These trends were observed for all the samples with different overlap distances (d = 50 nm, d = 60 nm). We note that the spectral separation between the resonance positions for both dipolar and Fano resonances, for two orthogonal polarizations, increases as the thickness of the metal film approaches the skin depth (≈25 nm at 1.8 μm). The influence of overlap distance on the optical spectra has been presented in prior work.[35]

To interpret the measured reflection spectra shown in Figure 2, full-field electromagnetic simulations are carried out using a Finite Element Method based software package, (COMSOL Multiphysics). The frequency-dependent dielectric permittivity of the gold film is described by Drude free electron model with a plasma frequency of 2175 THz and a collision frequency of 100 THz. The quartz substrate is characterized by a real-frequency independent dielectric constant of 1.45. In the simulation, Floquet periodic boundary conditions are applied for the transverse boundaries of the unit cell to replicate an infinite planar array of the unit cell. The port boundary conditions are used perpendicular to the *z-axis* to excite a plane wave from the top of the structure with a power of 1 W. The reflection ($R(\omega)$) spectrum is calculated from S-parameter. An overall good agreement is observed between simulated results and experimental measurements.

The simulated reflection spectra for *x*-polarization, for an overlap distance of 50 nm with different film thicknesses, are plotted in **Figure 3**. The reflection spectrum for the 50 nm thick film (black curve) shows a broad dip at 143 THz and a characteristic asymmetric sharp Fano dip at 180 THz. For the same structure with 100 and 200 nm film thicknesses, we find that the Fano resonances are shifted to higher frequencies (193 and 201 THz, respectively) without influencing the dipolar resonance frequency (143THz). The calculated quality factor ($Q = f_0 / \delta f$) of the Fano resonances for 50, 100, and 200 nm film thicknesses are Q = 36, Q = 33, and Q = 32, respectively. Thus, for a given annular and rectangular aperture array with a fixed overlap distance, film thickness can be effectively used as a control parameter to independently tune the spectral position of the Fano resonances in the optical spectrum. Simulated electric field plots in the *x*-*y* plane of the overlapping annular and rectangular aperture are shown in Figure 3b,c to understand the mode coupling. The electric field distribution for the super-radiant mode at 143 THz elucidates an azimuthally symmetric dipolar mode (m = 2), while the electric field plot for the dip at 193 THz indicates excitation of an asymmetrical quadrupole charge distribution in the annular aperture and a linear dipolar charge distribution in the rectangular slot, as shown in Figure 3. The interference between the linear dipole mode of rectangular aperture and the azimuthal quadrupole mode of annular aperture results in a pronounced Fano dip. It is important to note that the linear dipolar plasmon mode excited in the rectangular aperture is induced through the coherent near-field coupling between the directly excited plasmonic mode (super-radiant mode) of the annular aperture and the rectangular aperture. The second Fano dip in the reflection spectrum at 256 THz belongs to the excitation of a quadrupolar plasmon mode (m = 4) supported by the annular aperture structure and a quadrupolar plasmon mode in the rectangular slot.

In **Figure 4**, we show the simulated reflection spectra obtained from the same structure for *y*-polarization with different metal thicknesses. The reflection spectrum for 50 nm thick film (black curve) shows a broad dip at 167 THz and a characteristic asymmetric line shaped Fano resonance dip at 182 THz. As the metal film thickness increases, the Fano resonances are blue-shifted in the reflection spectrum while the spectral position of the super-radiant (dipolar) plasmon mode is constant. The spectral position of the Fano resonance for 100 and 200 nm films is shifted to 193 and 201 THz, respectively. In the

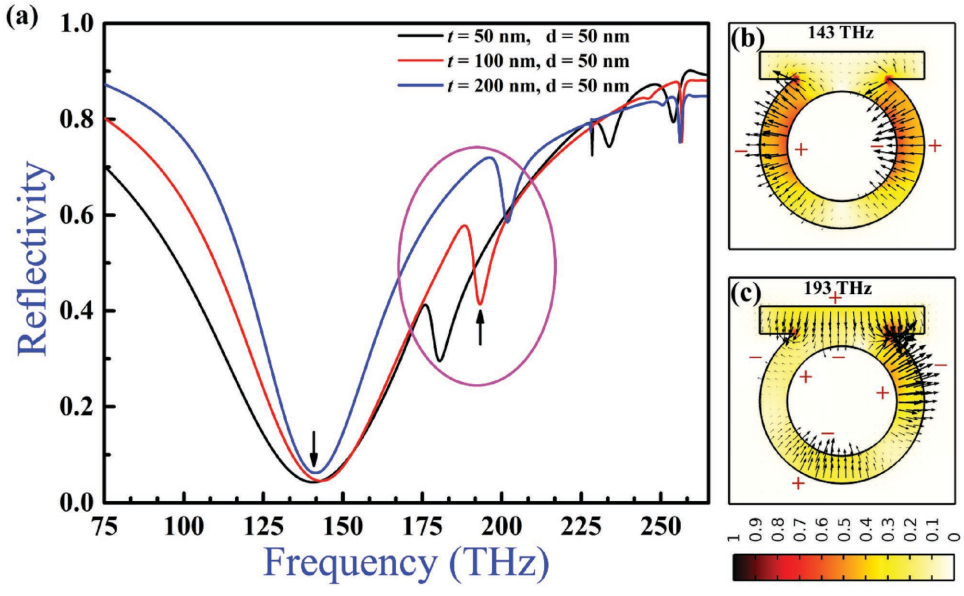

Figure 3. a) Calculated reflectance spectra for overlapping annular and rectangular aperture array milled in metal with different thicknesses with the electric field polarized along *x*-direction. The electric field distribution plots at the resonance dips (arrow marks in the simulated spectrum of metasurface with t = 100 nm and d = 50 nm) reveal the dipolar (m = 2) and quadrupolar (m = 4) charge distribution in the annular aperture as shown in panels (b) and (c). The arrows represent the vectors of electric field, and the color contour plot indicates the electric field norm.

Adv. Optical Mater. 2016,
DOI: 10.1002/adom.201600417

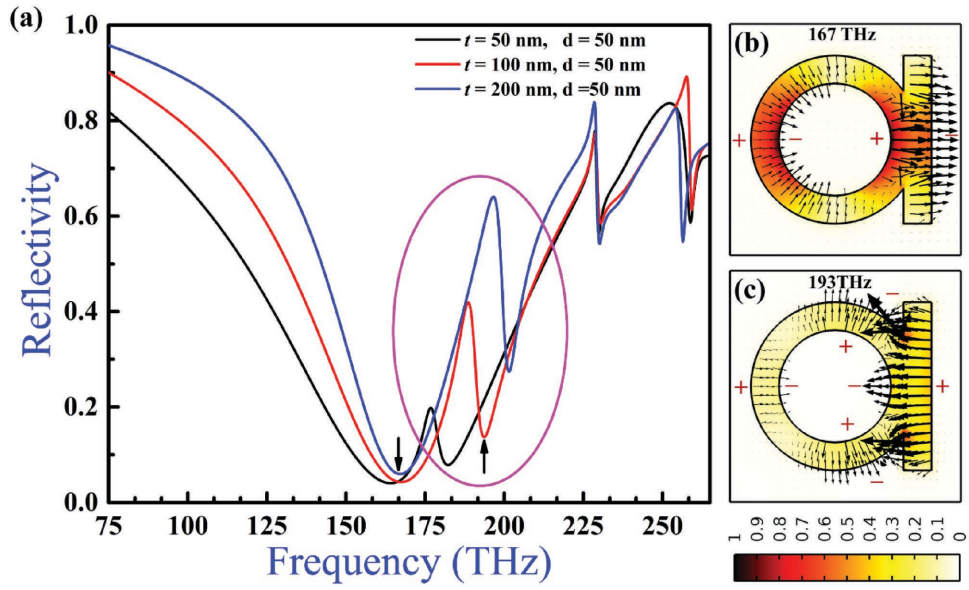

Figure 4. a) Calculated reflectance spectra for overlapping annular and rectangular aperture array milled in metal with different thickness with the electric field polarized along *y*-direction. The arrow marks in the simulated spectrum of the metasurface with $t = 100$ nm and $d = 50$ nm, correspond to the frequencies of field distribution plots shown in panels (b) and (c). The electric field distribution plots indicate the dipolar ($m = 2$) and quadrupolar ($m = 4$) charge distribution in the annular aperture. The arrows represent the vectors of electric field, and the color contour plot indicates the electric field norm.

case of *y*-polarization, not only the spectral position of the Fano resonance changes but also the amplitude of the resonance is considerably modified. The calculated quality factors of the Fano resonances for 50, 100, and 200 nm film thickness are $Q = 26$, $Q = 22$, and $Q = 21$, respectively. As seen from the electric field plots for the *x*-polarization, the Fano resonances for the *y*-polarization are excited due to interference of the quadrupolar resonance of the annular aperture with the directly excited dipolar resonance of the rectangular aperture.

To understand the origin of the spectral shift of the Fano resonances, we plot the simulated reflectance spectra obtained from the individual annular aperture array and rectangular aperture array milled in 50, 100, and 200 nm thick metal films in **Figure 5**. The simulated reflectance spectra for the annular aperture array show a broad dip at 164 THz, which is independent of the metal film thickness; however, the line-width of the resonance decreases with increasing metal film thickness. The broadening of the resonance for smaller film thickness is most likely from the higher loss of thinner metal films. Baida et al. have carried out a detailed numerical analysis of the thickness-dependent resonant transmission properties of the annular aperture arrays. Their finite difference time domain simulation shows that a guided mode in the sub-wavelength coaxial structure is responsible for the large transmission. The fundamental mode of a annular aperture guide in a PEC is the TE_{11} mode, which has a cutoff wavelength: $\lambda^{c}_{TE_{11}} \approx \pi^{*}(R_0 + R_i)$. For the annular aperture guide in a real metal, the cutoff wave is slightly modified: $\lambda^{c}_{TE_{11}} \sim n^{*}\pi^{*}(R_0 + R_i)$, where n_{sub} is the refractive index of the substrate.[36–39] In a further study, Haftel et al. investigated the role of a "cylindrical" surface plasmons (CSPs) on cylindrical interfaces of annular apertures. They found that CSP transmission peak occurs whenever a cylindrical surface plasmon (CSP) $n = 1$ normal mode is supported for an isolated aperture when the longitudinal wave number k_z satisfies $k_z t = n\pi$, where n is an integer and 't' is the thickness of the film. Thus, these are propagating (predominantly TE_{11}) modes, not evanescent, through the aperture. For an optically thin film, i.e., film thickness < wavelength, the peak at the longest wavelength is for $n = 0$ and corresponds to $k_z = 0$, i.e., at the cutoff wavelength of TE_{11} mode, and its position is independent of metal thickness 't' as we observed in our case.[40,41]

In the case of rectangular aperture array, the simulated reflectance spectra show strong film thickness dependence of the resonance position. As shown in Figure 5b, the spectral position of the dipole resonance changes from 154, 164 to 171 THz as the metal film thickness increases from 50, 100 to 200 nm, respectively. Degiron et al. have studied the role of the aperture depth on the transmission of light through sub-wavelength holes in free-standing films.[42] They found two transmission regimes for sub-wavelength hole arrays depending on the aperture depth. For an optically thin film, i.e., film thickness < wavelength, SPs excited on the two surfaces couple via evanescent waves leading to the resonant passage of light through the array. They observed that the resonant peak shifts and broadens with decreasing film thickness in this regime as noted in our case.[42,43] For deeper holes, the SP modes of the two interfaces are uncoupled and the transmission falls exponentially as the film gets thicker. The transition between the two regimes occurs at a hole depth found to be roughly three times the effective skin depth of the metal film.

3. Conclusion

In summary, we introduced a simple method to independently control the spectral position of both the super-radiant and

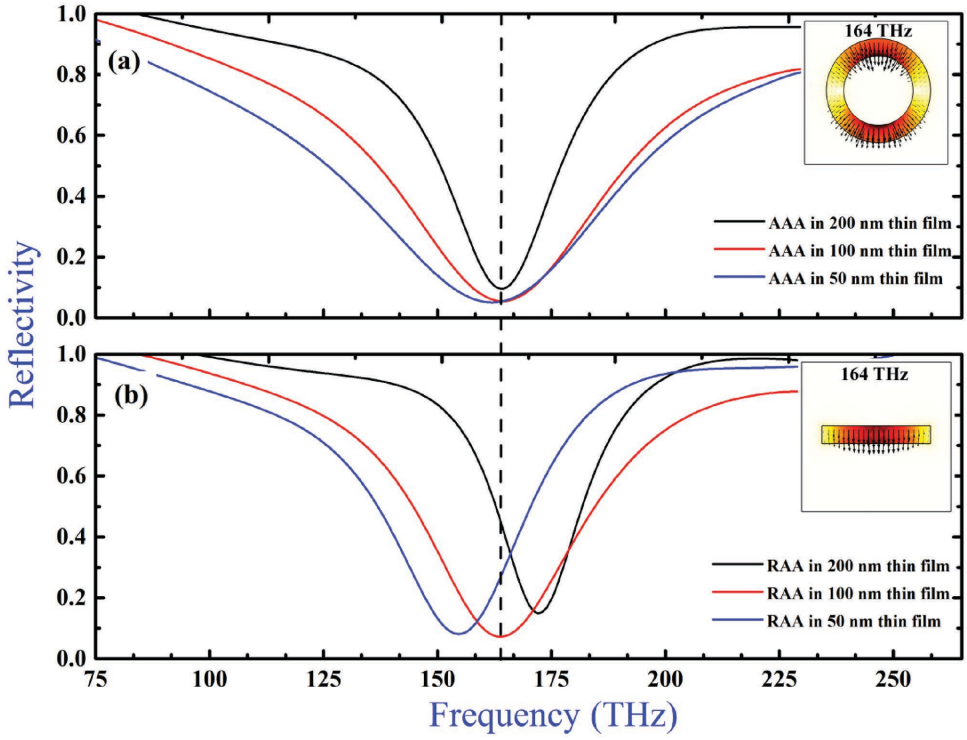

Figure 5. Calculated reflectance spectra for the a) annular aperture array and b) rectangular aperture array in 50, 100, and 200 nm thick metal films with the electric field polarized perpendicular to the length of the rectangular aperture. The inset plots show the electric field distribution in the individual annular and rectangular apertures at the resonance dip.

sub-radiant plasmon modes of the Fano resonances excited in the metal film perforated with a 2D square array of overlapping annular and rectangular apertures. Our experimental and numerical study shows that the spectral position of the Fano resonance is extremely sensitive to the thickness of the metal film and can be tuned over a wide spectral range without influencing the spectral position of the fundamental plasmon mode. We showed that the complete spectral control of Fano resonances is enabled by proper choice of resonators that have contrasting thickness-dependent optical responses. Our study demonstrates a new method to tune the spectral position of Fano resonance that can be used, for instance, to match the specific molecular vibrational fingerprints for ultra-sensitive single molecule detection.

Acknowledgements

The authors acknowledge NTU startup Grant No. M4081282, MOE Tier 1 Grant No. M4011362, and MOE Grant numbers MOE2011-T3-1-005 and MOE2015-T2-2-103 for the funding of this research.

Received: May 31, 2016
Revised: July 13, 2016
Published online:

[1] B. E. Sernelius, *Surface Modes in Physics*, Wiley-VCH, Berlin **2001**.
[2] S. A. Maier, *Plasmonics: Fundamentals And Applications*, Springer, New York **2007**.
[3] S. Enoch, N. Bonod, *Plasmonics: From Basics to Advanced Topics*, Springer, Berlin **2012**.
[4] S. Eustis, M. A. El-Sayed, *Chem. Soc. Rev.* **2006**, *35*, 209.
[5] K. A. Willets, R. P. Van Duyne, *Rev. Phys. Chem.* **2007**, *58*, 267.
[6] J. J. Mock, *J. Chem. Phys.* **2002**, *116*, 6755.
[7] H. Xu, E. J. Bjerneld, M. Käll, L. Börjesson, *Phys. Rev. Lett.* **1999**, *83*, 4357.
[8] P. Anger, P. Bharadwaj, L. Novotny, *Phys. Rev. Lett.* **2006**, *96*, 113002.
[9] J. N. Anker, W. P. Hall, O. Lyanders, N. C. Shah, J. Zhao, R. P. Van Duyne, *Nat. Mater.* **2008**, *7*, 442.
[10] F. Wang, Y. Ron Shen, *Phys. Rev. Lett.* **2006**, *97*, 206806.
[11] G. Sun, J. B. Khurgin, A. Bratkovsky, *Phys. Rev. B.* **2011**, *84*, 045415.
[12] E. Prodan, C. Radloff, N. J. Halas, P. Nordlander, *Science* **2003**, *302*, 4119.
[13] U. Fano, *Phys. Rev.* **1961**, *124*, 1866.
[14] B. Luk'yanchuk, N. I. Zheludev, S. A. Maier, N. J. Halas, P. Nordlander, H. Giessen, C. T. Chong, *Nat. Mater.* **2010**, *9*, 707.
[15] A. E. Miroshnichenko, S. Flach, Y. S. Kivshar, *Rev. Mod. Phys.* **2010**, *82*, 2257.
[16] A. B. Khanikaev, C. Wu, G. Shvets, *Nanophotonics* **2013**, *2*, 247.
[17] V. A. Fedotov, M. Rose, S. L. Prosvirnin, N. Papasimakis, N. I. Zheludev, *Phys. Rev. Lett.* **2007**, *99*, 147401.
[18] F. Hao, P. Nordlander, Y. Sonnefraud, P. Van Dorpe, S. A. Maier, *ACS Nano* **2009**, *3*, 643.
[19] A. E. Cetin, H. Altug, *ACS Nano* **2012**, *6*, 9989.
[20] Y. H. Fu, J. B. Zhang, Y. F. Yu, *ACS Nano* **2012**, *6*, 5130.
[21] M. Hentschel, M. Saliba, R. Vogelgesang, H. Giessen, A. P. Alivisatos, N. Liu, *Nano Lett.* **2010**, *10*, 2721.
[22] H. L. Liu, E. S. P. Leong, Z. L. Wang, G. Y. Si, L. J. Zheng, Y. J. Liu, C. Soci, *Adv. Opt. Mater.* **2013**, *1*, 978.

[23] J. A. Fan, K. Bao, C. Wu, J. Bao, R. Bardhan, N. J. Halas, V. N. Manoharan, G. Shvets, P. Nordlander, F. Capasso, *Nano Lett.* **2010**, *10*, 4680.
[24] B. Gallinet, O. J. F. Martin, *ACS Nano* **2011**, *5*, 8999.
[25] M. Gupta, V. Savinov, N. Xu, L. Cong, G. Dayal, S. Wang, W. Zhang, N. I. Zheludev, R. Singh, *Adv. Mater.* **2016**, DOI: 10.1002/adma.201601611.
[26] Y. K. Srivastava, M. Manjappa, L. Cong, W. Cao, I. Al-Naib, W. Zhang, R. Singh, *Adv. Opt. Mat.* **2015**, *4*, 457.
[27] R. Singh, I. Al-Naib, M. Koch, W. Zhang, *Opt. Exp.* **2011**, *19*, 6312.
[28] L. Cong, S. Tan, R. Yahiaoui, F. Yan, W. Zhang, R. Singh, *Appl. Phys. Lett.* **2015**, *106*, 031107.
[29] S.-D. Liu, E. S. P. Leong, G.-C. Li, Y. Hou, J. Deng, J. H. Teng, H. C. Ong, D. Y. Lei, *ACS Nano* **2016**, *10*, 1442.
[30] N. Verellen, P. V. Dorpe, C. Huang, K. Lodewijks, G. A. E. Vandenbosch, L. Lagae, V. V. Moschalkov, *Nano Lett.* **2011**, *11*, 391.
[31] Y. Zhan, D. Y. Lei, X. Li, S. A. Maier, *Nanoscale* **2014**, *6*, 4705.
[32] F. Hao, Y. Sonnefraud, P. Van Dorpe, S. A. Maier, N. J. Halas, P. Nordlander, *Nano Lett.* **2008**, *8*, 3983.
[33] M. Hentschel, M. Saliba, R. Vogelgesang, H. Giessen, A. P. Alivisatos, N. Liu, *Nano Lett.* **2010**, *10*, 2721.
[34] R. Singh, C. Rockstuhl, F. Lederer, W. Zhang, *Phys. Rev. B* **2009**, *79*, 085111.
[35] G. Dayal, X. Y. Chin, C. Soci, R. Singh, *Adv. Opt. Mater.* **2016**, DOI: 10.1002/adom.201600356.
[36] F. I. Baida, D. Van Labeke, *Opt. Commun.* **2002**, *209*, 17.
[37] A. Moreau, G. Granet, F. I. Baida, D. Van Labeke, *Opt. Express* **2003**, *11*, 1131.
[38] F. I. Baida, A. Belkhir, D. Van Labeke, O. Lamrous, *Phys. Rev. B* **2006**, *74*, 205419.
[39] W. Fan, S. Zhang, B. Minhas, K. J. Malloy, S. R. J. Brueck, *Phys. Rev. Lett.* **2005**, *94*, 033902.
[40] M. I. Haftel, C. Schlockermann, G. Blumberg, *Phys. Rev. B.* **2006**, *74*, 235405.
[41] S. M. Orbons, A. Roberts, D. N. Jamieson, M. I. Haftel, C. Schlockermann, D. Freeman, B. Luther-Davies, *Appl. Phys. Lett.* **2007**, *90*, 251107.
[42] A. Degiron, H. J. Lezec, W. L. Barnes, T. W. Ebbesen, *Appl. Phys. Lett.* **2002**, *81*, 4327.
[43] T. W. Ebbesen, H. J. Lezec, H. F. Ghaemi, T. Thio, P. A. Wolff, *Nature* **1998**, *391*, 667.